Tuning of multi-instabilities in organic alloy, [(EDO-TTF) 1-x(MeEDO-TTF)x]2PF6

ARTICLE *in* CHEMISTRY OF MATERIALS · MAY 2010

Impact Factor: 8.35 · DOI: 10.1021/cm100051b

CHEMISTRY OF MATERIALS
Article

Chem. Mater. **2010,** *22,* 3121–3132 3121
DOI:10.1021/cm100051b

Tuning of Multi-Instabilities in Organic Alloy, $[(EDO\text{-}TTF)_{1-x}(MeEDO\text{-}TTF)_x]_2PF_6$

Tsuyoshi Murata,*[,†,‡] Xiangfeng Shao,[†] Yoshiaki Nakano,[†] Hideki Yamochi,*[,†] Mikio Uruichi,[§] Kyuya Yakushi,[§] Gunzi Saito,[∥] and Koichiro Tanaka[⊥,#,▽]

[†]*Research Center for Low Temperature and Materials Sciences, Kyoto University, Sakyo-ku, Kyoto 606-8501, Japan,* [‡]*Department of Chemistry, Graduate School of Science, Osaka University, Toyonaka, Osaka 560-0043, Japan,* [§]*Institute for Molecular Science, Okazaki, Aichi 444-8585, Japan,* [∥]*Research Institute, Meijo University, Tempaku-ku, Nagoya 468-8502, Japan,* [⊥]*Department of Physics, Graduate School of Science, Kyoto University, Sakyo-ku, Kyoto 606-8502, Japan,* [#]*Core Research for Evolutional Science and Technology (CREST), Japan Science and Technology Agency (JST), Kawaguchi, Saitama 332-0012, Japan, and* [▽]*Institute for Integrated Cell-Material Sciences (iCeMS), Kyoto University, Sakyo-ku, Kyoto 606-8501, Japan*

Received January 7, 2010. Revised Manuscript Received April 7, 2010

Electrocrystallization of a mixture of 4,5-ethylenedioxytetrathiafulvalene (EDO-TTF) and 4,5-ethylenedioxy-4′-methyltetrathiafulvalene (MeEDO-TTF) yielded alloyed salts, $[(EDO\text{-}TTF)_{1-x}(MeEDO\text{-}TTF)_x]_2PF_6$ (x = mole fraction of MeEDO-TTF). EDO-TTF rich alloys ($x \leq 0.5$) were isostructural to $(EDO\text{-}TTF)_2PF_6$, the metal−insulator transition of which is caused by the cooperation of Peierls, anion-ordering, and charge-ordering mechanisms. Incorporation of MeEDO-TTF into $(EDO\text{-}TTF)_2PF_6$ extended the donor−anion distance to weaken donor−anion interactions, while donor−donor interactions within the conduction layer remained the same magnitudes to those of $(EDO\text{-}TTF)_2PF_6$ having a quasi-one-dimensional electronic structure. These alloys showed a metallic behavior or nearly constant resistivity around room temperature, and their transport properties strongly depended on x value. $x \leq 0.13$ alloys showed a sharp metal−insulator transition due to Peierls instability and anion-ordering, and transition temperature decreased as x increased. Although charge-ordering in the donor column was also elucidated for the insulator phase of $x \leq 0.05$ alloys, uniform +0.5 charge of donor molecules was preserved in the low-temperature phase of $x = 0.13$ alloy. In the case of the $x \sim 0.5$ alloy, any abrupt anomalies were not detected down to low temperature, while broad resistivity minimum was observed at 200−270 K. $x \geq 0.9$ alloys were isostructural to $(MeEDO\text{-}TTF)_2PF_6$, which forms a two-dimensional donor layer. Similar to $(MeEDO\text{-}TTF)_2PF_6$, MeEDO-TTF rich alloys exhibited a semiconductor-to-semiconductor phase transition. The transition became gradual, and the transition temperature was suppressed with decreasing x value. Raman spectra indicated that nearly localized and distinct charge-disproportionated states, which are observed in the high- and low-temperature phases of pristine $(MeEDO\text{-}TTF)_2PF_6$, respectively, coexist in the high-temperature phase.

Introduction

Tetrathiafulvalene (TTF) has been the most actively studied molecular system in the research field of organic conductors since the discovery of the first organic metal (TTF)(TCNQ) complex (TCNQ = tetracyanoquinodimethane).[1] Charge-transfer complexes of TTF derivatives have afforded numerous organic semiconductors, metals, and superconductors, and furthermore, their anisotropic electronic structures having flexible molecular and crystal structures have provided many fascinating phase transition systems.[2−4]

Scheme 1

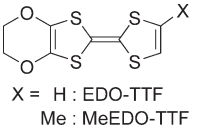

We have recently discovered a peculiar phase transition system, $(EDO\text{-}TTF)_2PF_6$ (EDO-TTF = ethylenedioxy-TTF, Scheme 1), which exhibits a metal−insulator (M-I) thermal transition at near room temperature (T_{MI} = 279.0 K) caused by the cooperation of three mechanisms, Peierls instability, anion-ordering (AO), and charge-ordering (CO).[5−7] Nearly uniform donor stack showing a

*To whom correspondence should be addressed. Tel: (+81)-75-753-4069. Fax: (+81)-75-753-4069. E-mail: tmurata@chem.sci.osaka-u.ac.jp (T.M.), yamochi@kuchem.kyoto-u.ac.jp (H.Y.).

(1) Ferraris, J.; Cowan, D. O.; Walatka, V., Jr.; Perlstein, J. H. *J. Am. Chem. Soc.* **1973**, *95*, 948–949.
(2) For the comprehensive review, see Chem. Rev. **2004**, *104* (11).
(3) Saito, G.; Yoshida, Y. *Bull. Chem. Soc. Jpn.* **2007**, *80*, 1–137.
(4) Yamada, J., Sugimoto, T., Eds. *TTF Chemistry: Fundamentals and Applications of Tetrathiafulvalene*; Kodansha Springer: Tokyo, 2004.
(5) Ota, A.; Yamochi, H.; Saito, G. *J. Mater. Chem.* **2002**, *12*, 2600–2602.

Published on Web 04/28/2010

quasi-one-dimensional Fermi surface in the high-temperature (HT) phase changes to a strongly tetramerized form having a [0, +1, +1, 0] CO pattern in the low-temperature (LT) phase. We have investigated the effects of external stimuli and chemical modifications on this multi-instability system. In the conductivity measurement of (EDO-TTF)$_2$PF$_6$ under uniaxial strain, the compression along the interlayer direction extraordinarily enhanced the M-I transition (T_{MI} > 340 K at 2−4 kbar) compared to that in the intralayer constrictions.[8] Along with the contraction of donor−anion distances associated with the phase transition from HT to LT phase at ambient pressure,[7] this observation indicates the importance of the interaction between donor and anion molecules. Deuteration of the vinyl group of EDO-TTF affected not only the C−H (D) vibration but also on the skeletal ones of the π-electron system in the IR and Raman spectra, and the deuterated salt showed a higher M-I transition temperature than that of the pristine salt (ΔT_{MI} = 2−3 K).[9] Increase of the anion-size in (EDO-TTF)$_2$X (for X, PF$_6$ < AsF$_6$ < SbF$_6$) significantly suppressed the M-I transition (AsF$_6$, T_{MI} = 270.8 K; and SbF$_6$, T_{MI} = 242 K).[10] Not only in the static properties mentioned above but also in the dynamic process, (EDO-TTF)$_2$PF$_6$ showed a peculiar feature. By irradiating a pulsed laser light, the LT phase showed an ultrafast and highly efficient photoinduced phase transition,[11,12] which is regarded as a potential phenomenon for the development of an ultrafast photo switching system. In this dynamic process, the strong electron−lattice interaction plays an important role as evidenced by the observation of coherent peaks. Because of the gigantic response to external stimuli, this material attracts much attention in the new scientific field on the nonequilibrium state of solids.[13]

These peculiar features of (EDO-TTF)$_2$PF$_6$ inspired us to investigate radical cation salts of EDO-TTF analogues. Monomethyl substituted EDO-TTF (MeEDO-TTF, Scheme 1),[14] possessing a similar π-electron system and slightly bigger molecular size (~1.2 Å longer along the molecular long axis) than those of EDO-TTF, yielded charge-transfer complexes exhibiting different features from those of EDO-TTF. MeEDO-TTF salts formed various types of molecular packing, which strongly affected their electronic structures. The head-to-tail stack of donor molecules provided quasi-one-dimensional systems or localized electronic structures in donor multimers,[15] while the head-to-head stack formed two-dimensional systems with relatively weak donor−donor interactions.[16,17] Among the latter cases, (MeEDO-TTF)$_2$X (BF$_4$ and ClO$_4$) showed a metallic behavior down to cryogenic temperature.[16] The slightly bulkier anion, PF$_6$ provided three kinds of 2:1 salts. One of the modifications whose crystal structure was isostructural to those of (MeEDO-TTF)$_2$X (BF$_4$ and ClO$_4$) exhibited a semiconductor-to-semiconductor first-order phase transition associated with the modulation of charge-disproportionation (CD) and relative molecular orientation.[17] The CD states in HT and LT phases were assigned to nearly localized and distinct ones, respectively, though the crystal structure analyses could not detect the differently charged donor molecules in both phases. The charge on a donor molecule (site charge) was fluctuated especially in the HT phase, which resulted in the broadening of C=C stretching modes in the Raman spectra. The subtle balance between the neighboring site Coulomb interaction and intermolecular transfer integral is regarded as playing an important role in specifying the CD states of HT and LT phases, and the temperature dependence of the balance should be related to the phase transition.

The systematic modulation of crystal and electronic structures should derive fundamental information to clarify origins of the peculiar phase transitions of EDO-TTF and MeEDO-TTF salts and to achieve future materials design of phase transition systems. For the continuous modulation of band-filling,[18,19] intermolecular interactions,[20] etc., alloying a complex with foreign substances (conducting part having a similar structure or counterpart with different charge or size) is one of the convenient chemical methods. Fortunately, it was proved that the solid solution of EDO-TTF and MeEDO-TTF salts with PF$_6$ is available by the electrocrystallization of a mixture of EDO-TTF and MeEDO-TTF in the presence of PF$_6$ anion despite the differences in the crystal structures and physical properties between (EDO-TTF)$_2$PF$_6$ and (MeEDO-TTF)$_2$PF$_6$. The steric hindrance of the methyl

(6) Ota, A.; Yamochi, H.; Saito, G. *Synth. Met*. **2003**, *135−136*, 643–644.
(7) Aoyagi, S.; Kato, K.; Ota, A.; Yamochi, H.; Saito, G.; Suematsu, H.; Sakata, M.; Takaka, M. *Angew. Chem., Int. Ed*. **2004**, *43*, 3670–3673.
(8) Sakata, M.; Maesato, M.; Ota, A.; Yamochi, H.; Saito, G. *Synth. Met*. **2005**, *153*, 393–396.
(9) Nakano, Y.; Balodis, K.; Yamochi, H.; Saito, G.; Uruichi, M.; Yakushi, K. *Solid State Sci*. **2008**, *10*, 1780–1785.
(10) Nakano, Y.; Yamochi, H.; Saito, G.; Uruichi, M.; Yakushi, K. *J. Phys.: Conf. Ser*. **2009**, *148*, 012007/1–012007/4.
(11) Chollet, M.; Guerin, L.; Uchida, N.; Fukaya, S.; Shimoda, H.; Ishikawa, T.; Matsuda, K.; Hasegawa, T.; Ota, A.; Yamochi, H.; Saito, G.; Tazaki, R.; Adachi, S.; Koshihara, S. *Science* **2005**, *307*, 86–89.
(12) Onda, K.; Ogihara, S.; Yonemitsu, K.; Maeshima, N.; Ishikawa, T.; Okimoto, Y.; Shao, X.; Nakano, Y.; Yamochi, H.; Saito, G.; Koshihara, S. *Phys. Rev. Lett*. **2008**, *101*, 067403/1–067403/4.
(13) For the comprehensive review, see J. Phys.: Conf. Ser. **2009**, *148*.
(14) Miyazaki, A.; Enoki, T. *Synth. Met*. **2001**, *120*, 939–940.
(15) Shao, X.; Yoshida, Y.; Nakano, Y.; Yamochi, H.; Sakata, M.; Maesato, M.; Otsuka, A.; Saito, G.; Koshihara, S. *Chem. Mater*. **2009**, *21*, 1085–1095.
(16) Shao, X.; Nakano, Y.; Yamochi, H.; Dubrovskiy, A. D.; Otsuka, A.; Murata, T.; Yoshida, Y.; Saito, G.; Koshihara, S. *J. Mater. Chem*. **2008**, *18*, 2131–2140.
(17) Shao, X.; Nakano, Y.; Sakata, M.; Yamochi, H.; Yoshida, Y.; Maesato, M.; Uruichi, M.; Yakushi, K.; Murata, T.; Otsuka, A.; Saito, G.; Koshihara, S.; Tanaka, K. *Chem. Mater*. **2008**, *20*, 7551–7562. The Raman bands denoted as ν_{11}, ν_{10}, and ν_9, the main components of which are the C=C bond vibrations, were observed at 1533, 1624, and 1649, and 1415, 1531, and 1553 cm^{-1} for neutral and +1.0 charged MeEDO-TTF. It should also be noted that the anomalous shift of the ν_{11} mode was observed in (MeEDO-TTF)$_2$PF$_6$, the origin of which is assigned to the strong electron−vibration coupling.
(18) Mori, T. *Chem. Rev*. **2004**, *104*, 4947–4969 and references therein.
(19) Epstein, A. J.; Miller, J. S. In *The Physics and Chemistry of Low Dimensional Solids*; Alcacer, L., Ed.; D. Reidel: Dordrecht, The Netherlands, 1980; pp 339−351.
(20) (a) Kato, R.; Sawa, H.; Aonuma, S.; Tamura, M.; Kinoshita, M.; Kobayashi, H. *Solid State Commun*. **1993**, *85*, 831–835. (b) Bauer, D.; von Schütz, J. U.; Wolf, H. C.; Hünig, S.; Sinzger, K.; Kremer, R. K. *Adv. Mater*. **1993**, *5*, 829–834.

group is expected to weaken donor−anion interactions along the molecular long axis (perpendicular to the conduction layer). To clarify essential origins of the phase transitions of $(EDO\text{-}TTF)_2PF_6$ and $(MeEDO\text{-}TTF)_2PF_6$ and to tune their physical properties, we investigated alloys between these salts in a wide range of mole fractions. Here, we present the preparation, structural analyses, and physical properties of alloys: $[(EDO\text{-}TTF)_{1-x}(MeEDO\text{-}TTF)_x]_2PF_6$ (denoted hereafter as $(Me_xEDO\text{-}TTF)_2PF_6$, x is mole fraction of MeEDO-TTF).

Experimental Section

General Details. The supporting electrolytes of tetrabutylammonium (Bu_4N) and 1-butyl-3-methylimidazolium (BMI) PF_6 were purified by the recrystallization from EtOH and the treatment with charcoal in EtOH, respectively. EtOH for the electrocrystallization was distilled over Mg/I_2 and stored under nitrogen atmosphere. In an H-shaped cell with a glass frit separating two chambers, a mixture of EDO-TTF and MeEDO-TTF, and electrolyte were placed in the anodic and both chambers, respectively. After dissolving the donor and supporting electrolyte in EtOH under nitrogen, a constant current was applied between platinum electrodes with diameters of 2 and 1 mm for the anode and cathode, respectively. In a typical procedure, the donor (ca. 28 mg) and supporting electrolyte (ca. 250 mg for $(Bu_4N)PF_6$ or ca. 140 mg for $(BMI)PF_6$) were dissolved in 40 mL of EtOH. Electrooxidation applying a constant current of 1−2 μA for 1−2 weeks afforded the alloy as black elongated platelet crystals.

The electron impact mass spectra (EI-MS) were measured on pieces of a crystalline sample with Thermo Finngan Trace DSQ. Mole fraction of MeEDO-TTF in an alloy (x) was determined by the least-squares fitting of the observed spectrum of molecular ion peaks using m/z = 262, 263, and 264 for $(EDO\text{-}TTF)_2PF_6$ and m/z = 276, 277, and 278 for $(MeEDO\text{-}TTF)_2PF_6$. Experimental deviations of the x value were ±0.01 for one crystal and ±0.02 for one batch. It should be noted that the estimation of x values in this method should bear some systematic error since efficiencies of EDO-TTF and MeEDO-TTF molecules to produce molecular ions should be different from each other. Throughout this article, however, the x value obtained by ignoring this difference is regarded as the mole fraction. The x value of a crystal for the structural analysis or physical measurements is indicated by a numerical value when the EI-MS was carried out on the piece of the crystal examined, while a range of x values is indicated when the analysis was performed only for other crystals in the same batch as the crystal from which structural/physical data were obtained.

The resistivities were measured through the conventional four-probe method. Gold wires of ϕ = 10 μm were contacted with the surface of a sample by using gold paste (Tokuriki, 8560-1A). The magnetic properties were measured on single crystals through ESR (JEOL JESTE200 X-band ESR spectrometer with TE011 cavity) in the temperature range of 4−300 or 310 K. For each measurement of temperature dependence of ESR parameters, one piece of a single crystal was placed in the cavity. Raman spectra were measured on 180° back-reflecting geometry with Renishaw Ramanscope System-1000. The excitation wavelength was 633 nm (He−Ne line), and the incident light was polarized in the molecular short axis (a-axis for EDO-TTF rich alloys and b-axis for MeEDO-TTF rich alloys).

Intermolecular overlap integrals between HOMOs of donor molecules were calculated by means of the extended Hückel method on the basis of crystal structures. The tight-bind band calculation afforded a dispersion relation and Fermi surface under the assumption of $t = Es$, where t and s represent the transfer integrals and overlap integrals, respectively, and $E = -10$ eV. The ζ-parameters of atomic orbitals were taken from ref 21 for oxygen and from ref 22 for other atoms. The 3d orbitals of sulfur atoms were included in the calculation.

X-ray Structure Determination. The data were collected on an imaging plate type diffractometer (MacScience DIP-2020K) with graphite monochromated Mo Kα radiation. Temperature for X-ray data collection was controlled by an XR-CS10K cryostat (Japan Thermal Engineering). Structures were solved by a direct method of Shelxs-97[23] or SIR2004,[24] and refined by a full matrix least-squares method on F^2 by means of Shelxl-97.[25] All non-hydrogen atoms were refined anisotropically except for the disordered methyl and ethylene groups. Positional parameters of hydrogen atoms were calculated under a fixed C−H bond length of 1.00 Å with sp^2 or sp^3 configuration of the bonding carbon atoms. In the refinement procedures, isotropic temperature factors with magnitudes of 1.2 times those of the equivalent temperature factors of the bonding carbon atoms were applied for hydrogen atoms.

Methyl group of the donor molecule exhibited a positional disorder at two vinyl carbon atoms. Contribution of the methyl group was ignored for x = 0.03−0.22 alloys in the structural analyses, and the refinement was performed considering the donor as an EDO-TTF molecule. In the refinement of the x = 0.48 alloy, ignoring the methyl group, the differential synthesis afforded peak intensities of 1.37 and 2.24 for methyl groups close to the vinyl carbons, C8 and C10, respectively. Although the error was large, an uneven distribution of the methyl group on the vinyl carbons was expected. To avoid the interference with the temperature factor in the least-squares procedures, the site occupancy factor (s.o.f.) of each methyl group was refined assuming the magnitude of the temperature factor to be 1.25 times that of the bonding vinyl carbon. Also, the C−C bond length was restrained to 1.51 Å, and the sum of s.o.f. of the methyl carbon atoms on a vinyl group was fixed to be equal to the mole fraction of MeEDO-TTF determined by EI-MS. As a result, the s.o.f. for one of the methyl group sites became around twice that for another site; however, a detailed discussion about this ratio may be difficult due to the accuracy of the structural analysis. This method was also applied for the refinement of crystal structures of x = 0.37 and 0.44 alloys. The methyl group in $x \geq 0.91$ alloys were located on one side of the vinyl group, and the refinement was performed with the s.o.f. value of the methyl group estimated by the EI-MS spectrum.

Results and Discussions

Preparation of Alloys. Electrocrystallization of a mixture of EDO-TTF and MeEDO-TTF with an arbitrary ratio in EtOH including the $(Bu_4N)PF_6$ or $(BMI)PF_6$ electrolyte yielded alloys $(Me_xEDO\text{-}TTF)_2PF_6$ as black elongated platelet crystals. Table 1 summarizes the mixing ratio

(21) Summerville, R. H.; Hoffmann, R. *J. Am. Chem. Soc.* **1976**, *98*, 7240–7254.
(22) Mori, T.; Kobayashi, A.; Sasaki, Y.; Kobayashi, H.; Saito, G.; Inokuchi, H. *Bull. Chem. Soc. Jpn.* **1984**, *57*, 627–633.
(23) Sheldrick, G. M. SHELXS-97 A Program for Solution of Crystal Structures; University of Göttingen: Göttingen, Germany, 1997.
(24) Burla, M. C.; Caliandro, R.; Camalli, M.; Carrozzini, B.; Cascarano, G. L.; de Caro, L.; Giacovazzo, C.; Polidori, G.; Spagna, R. *J. Appl. Crystallogr.* **2005**, *38*, 381–388.
(25) Sheldrick, G. M. SHELXL-97 A Program for Crystal Structure Refinement; University of Göttingen: Göttingen, Germany, 1997.

Table 1. Mixing Ratio in the Electrocrystallization, Mole Fraction of MeEDO-TTF (x), Crystal Type (A, $(EDO\text{-}TTF)_2PF_6$; B, $(MeEDO\text{-}TTF)_2PF_6$), Room Temperature Conductivity (σ_{RT}), and Phase Transition Temperature (T_c) of $(Me_xEDO\text{-}TTF)_2PF_6$

batch	mixing ratio		yield	x[a]	crystal type	σ_{RT}, T_c[b]
	EDO-TTF	MeEDO-TTF				
1	28.3 mg (108 μmol)	0.24 mg (0.9 μmol)	18.3 mg	0.01−0.02	A	161 S cm^{-1}, 270 K
2	28.0 mg (107 μmol)	0.48 mg (1.7 μmol)	18.1 mg	0.02−0.04	A	5−113 S cm^{-1}, 262−264 K[c]
3	27.5 mg (105 μmol)	1.2 mg (4.3 μmol)	17.5 mg	0.05−0.06	A	49−147 S cm^{-1}, 242−243 K[c]
4	24.1 mg (91.8 μmol)	2.8 mg (10.1 μmol)	5.8 mg	0.13−0.15	A	16−58 S cm^{-1}, 188−193 K[c]
5	21.8 mg (83.1 μmol)	5.2 mg (18.8 μmol)	6.2 mg	0.22−0.26	A	14−63 S cm^{-1}, −[c,f]
6	18.8 mg (71.6 μmol)	8.4 mg (30.4 μmol)	4.9 mg	0.35−0.37	A	56 S cm^{-1}, −[f]
7	15.5 mg (59.1 μmol)	10.8 mg (39.1 μmol)	5.6 mg	0.42−0.44	A	13 S cm^{-1}, −[f]
8[d]	4.7 mg (17.9 μmol)	4.8 mg (17.4 μmol)	0.7 mg	0.48−0.51	A	48 S cm^{-1}, −[f]
9[d]	26.2 mg (99.8 μmol)	28.0 mg (101 μmol)	9.8 mg	0.52−0.55	A	−[g]
10[e]	12.0 mg (45.7 μmol)	16.2 mg (58.6 μmol)	6.7 mg	0.51−0.55	A	87−99 S cm^{-1}, −[c,f]
				0.91−0.94	B	2 S cm^{-1}, 284 K
11	9.3 mg (35.4 μmol)	19.2 mg (69.5 μmol)	6.5 mg	0.92−0.94	B	4 S cm^{-1}, 291 K
12	5.4 mg (20.6 μmol)	21.2 mg (76.7 μmol)	6.7 mg	0.97	B	1 S cm^{-1}, 298 K

[a] x values were determined by EI-MS spectra. Measurements were performed for several crystals for each batch. [b] Room temperature conductivity and phase transition temperature, respectively, the former of which strongly depended on crystal quality. T_c was determined by the on-set value of phase transition in the conductivity measurement, the x value of each crystal for which was determined individually unless otherwise noted. [c] Ranges of the values were presented when the measurements were performed for several crystals from one batch. [d] 91.0 and 500 mg of $(Bu_4N)PF_6$ in 18 and 100 mL of EtOH were used for batches 8 and 9, respectively. For other batches, see Experimental Procedures section. [e] Two kinds of crystals ($(EDO\text{-}TTF)_2PF_6$ (A) and $(MeEDO\text{-}TTF)_2PF_6$ (B) types) were obtained from the same batch. [f] Distinct phase transition was not observed. [g] Not measured.

of two donors, the mole fraction of MeEDO-TTF (x) in the crystal obtained, the crystal type, and the transport properties of the resulting alloys. The alloys were categorized into two types according to their crystal structures: isostructural to $(EDO\text{-}TTF)_2PF_6$ or $(MeEDO\text{-}TTF)_2PF_6$ (types A and B in Table 1, respectively). Single crystals suitable for the measurements from a MeEDO-TTF excess mixture (type B) were obtained only in the presence of $(BMI)PF_6$ (batches 10−12), which is reminiscent of the preparation of pristine $(MeEDO\text{-}TTF)_2PF_6$.[17] The mole fraction of MeEDO-TTF (x) in an alloy was determined by comparing the intensities of molecular ion peaks in EI-MS spectra as described in Experimental Section. Mole fractions of MeEDO-TTF in alloys of $x \leq 0.5$ were in good agreement with the mixing ratios in preparation, while alloys prepared from MeEDO-TTF excess mixtures (EDO-TTF/MeEDO-TTF < 1) had x values ($x \geq 0.91$) much larger than that expected from the mixing ratios (Table 1). From the solution of the EDO-TTF/MeEDO-TTF = 4:6 mixture including $(BMI)PF_6$ (batch 10 in Table 1), two kinds of crystals having needle-like (x = 0.51−0.55, type A) and elongated plate (x = 0.91−0.94, type B) shapes were obtained (Figure S1c, Supporting Information). These crystals were characterized as $(EDO\text{-}TTF)_2PF_6$ and $(MeEDO\text{-}TTF)_2PF_6$ types, respectively, by the X-ray diffraction measurement. Appearances of the alloys of $x \leq 0.5$ and $x \geq 0.91$ were very similar to those of pristine $(EDO\text{-}TTF)_2PF_6$ and $(MeEDO\text{-}TTF)_2PF_6$, respectively (Figure S1, Supporting Information). The most developed face of the former salt showed a distorted hexagonal shape or a pentagonal one due to the crack of crystals, while the latter salt was obtained as plates with a parallelepiped face often having concave and/or convex short sides(s).

1. EDO-TTF Rich Salts ($x \leq 0.5$). *Crystal Structures.* Crystallographic data of selected alloys are listed in Table 2 with the measurement temperatures (those of all measurements are summarized in Tables S1−S7, Supporting Information). Crystal structures of alloys at 300 K or room temperature were isostructural to that of $(EDO\text{-}TTF)_2PF_6$ in the HT phase. Although the b-axis length (//donor stacking direction) did not show a distinct difference (7.343(0.6) Å for $x = 0$ and 7.355(2) Å for $x = 0.48$), the c-axis length (nearly parallel to the molecular long axis) obviously became longer (11.944(1) Å for $x = 0$, and 12.258(3) Å for $x = 0.48$), indicating the steric effect of the methyl group to separate donor and anion layers. The asymmetric unit of the crystals contained one donor molecule and a half of the PF_6 anion showing a rotational disorder. No diffuse scattering corresponding to the superlattice of different kinds of donor molecules and/or anion orientations within our experimental sensitivity was observed. This means that EDO-TTF and MeEDO-TTF distributed randomly in the donor sites. Furthermore, the methyl group exhibited a positional disorder on the vinyl group judging from the peak intensities in differential synthesis. The donor molecules formed a weakly dimerized one-dimensional column along the b-axis with a head-to-tail stacking (Figure 1a). The columns were connected through S···S atomic contacts along the a-axis to form a conducting layer parallel to the ab plane (Figure 1b). The intermolecular overlap integrals calculated by the extended Hückel method were almost identical to those of $(EDO\text{-}TTF)_2PF_6$ ($s_1 = 27.4$, $s_2 = 27.3$, $p_1 = -6.3$, $p_2 = 2.3$, $t_1 = 1.6 \times 10^{-3}$)[5] and varied slightly according to x values (Table S10, Supporting Information). The tight-bind band calculation of the donor layer afforded a quasi-one-dimensional Fermi surface which is very similar to that of the HT phase of $(EDO\text{-}TTF)_2PF_6$ (Figure 1c).

In the low-temperature region, the alloys with $x \leq 0.13$ showed cell doubling along the diagonal direction of the ab plane in the HT phase. The LT phase structures were also isostructural to that of pristine $(EDO\text{-}TTF)_2PF_6$ in the LT phase. Two donor molecules and one PF_6 anion were crystallographically unique. The rotational disorder of the PF_6 anion observed in the HT phase was significantly

Table 2. Crystallographic Data of EDO-TTF Rich Alloys at 300 and 150 K[a,b]

	x = 0.03 (batch 2)		x = 0.05 (batch 3)		x = 0.13 (batch 4)		x = 0.48 (batch 8)	
T (K)	300 K	150 K	300 K	150 K	300 K	150 K	300 K	150 K
crystal system	triclinic	triclinic	triclinic	triclinic	triclinic	triclinic	triclinic	triclinic
space group	$P\bar{1}$	$P\bar{1}$	$P\bar{1}$	$P\bar{1}$	$P\bar{1}$	$P\bar{1}$	$P\bar{1}$	$P\bar{1}$
a (Å)	7.203(1)	9.760(3)	7.205(0.7)	9.778(1)	7.211(0.6)	9.552(1)	7.286(1)	7.230(0.9)
b (Å)	7.349(0.8)	11.083(2)	7.350(2)	11.065(2)	7.354(1)	10.815(0.9)	7.355(2)	7.261(1)
c (Å)	11.965(2)	11.203(3)	11.982(2)	11.268(2)	12.022(2)	11.950(1)	12.258(3)	12.169(2)
α (deg)	93.495(8)	101.66(2)	93.527(9)	101.666(8)	93.608(6)	101.836(6)	93.91(1)	93.310(9)
β (deg)	75.196(7)	100.22(1)	75.232(9)	100.121(8)	75.377(7)	99.191(6)	75.50(1)	75.70(1)
γ, deg	97.368(8)	88.72(2)	97.288(9)	88.786(8)	97.105(8)	90.420(7)	96.69(1)	96.155(8)
V (Å^3)	607.0(2)	1167.9(5)	608.3(2)	1175.2(3)	611.8(1)	1191.7(2)	631.1(2)	615.2(2)
Z	1	2	1	2	1	2	1	1
no. of unique refln.	2176	3393	2170	4150	2160	4278	2223	2199
no. of used refln.	1585	2890	1513	2805	1753	2590	1354	1572
no. of params	188	316	188	316	188	335	194	194
R ($I > 2\sigma(I)$)	0.0542	0.0471	0.0541	0.0649	0.0667	0.0825	0.0750	0.0529
$wR2$ (all data)	0.1635	0.1339	0.1797	0.1941	0.1951	0.2937	0.2318	0.1635
GOF	1.092	1.104	1.076	1.040	1.195	1.089	1.001	1.080

[a] x value for each crystal was determined by EI-MS measurement. [b] Data not listed here are summarized in Supporting Information.

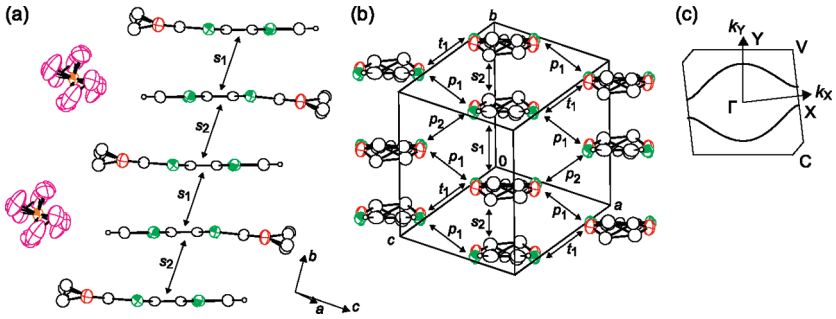

Figure 1. (a) One-dimensional donor stacking column and neighboring anions of $(Me_xEDO\text{-}TTF)_2PF_6$ (x = 0.05 (batch 3)) at 300 K. Each two sites were assigned for every ethylene carbon and fluorine atom to express the structural disorder. (b) Donor layer viewed along the molecular long axis of the donor molecule. Because of too small contributions, those of the methyl groups were ignored in the structural analysis. Letters in (b) present intermolecular overlap integrals calculated by the extended Hückel method: $s_1 = 27.6$, $s_2 = 26.9$, $p_1 = -6.3$, $p_2 = 2.2$, and $t_1 = 1.4 \times 10^{-3}$; see Table S10, Supporting Information. (c) Calculated Fermi surface of this alloy at 300 K.

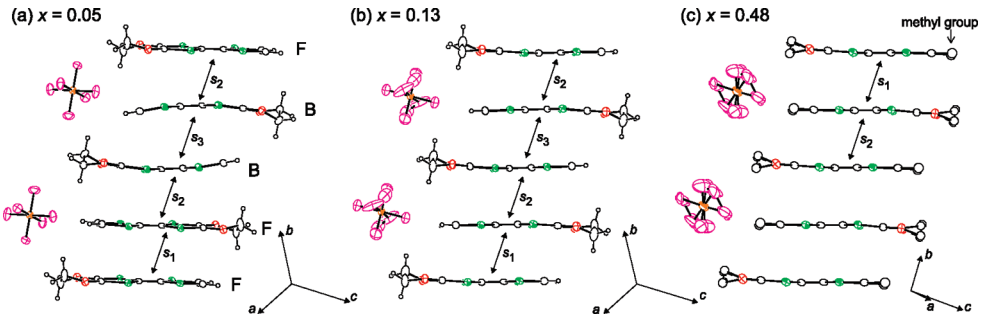

Figure 2. One-dimensional stacking column of alloys of (a) x = 0.05 (batch 3), (b) x = 0.13 (batch 4), and (c) x = 0.48 (batch 8) at 150 K. Letters present intermolecular overlap integrals calculated by the extended Hückel method (see Tables S10 and S11, Supporting Information). Because of too small contributions, those of methyl groups were ignored in the structural analyses for the x = 0.05 and 0.13 alloys. It should be noted that the x = 0.48 alloy did not exhibit any structural transitions (cell doubling) down to 150 K.

suppressed in the LT phase, although the disorder was partly preserved at 150 K in the x = 0.13 alloy (Figure 2a and b). In the x = 0.03 and 0.05 (batches 2 and 3) alloys, two crystallographically unique donor molecules showed different molecular shapes with nearly flat (**F**: dihedral angles between the best planes defined by terminal $C_2O_2S_2$ and central C_2S_4 and that by central C_2S_4 and terminal C_2S_2 moieties are 1.1−1.5 and 2.5° at 150 K, respectively) and bent (**B**: 10.0 and 7.9−8.0° at 150 K) structures (Figure 2a). This feature implies the CO state of donor molecules as observed in $(EDO\text{-}TTF)_2PF_6$, where the **F** and **B** molecules possess charges close to +1 and 0, respectively.[7] In fact, the significant differences in the central C=C bond lengths of the **F** and **B** donor molecules, 1.371(8)−1.377(6) and 1.341(6)−1.355(8) Å at 150 K, respectively, also suggest that the charges are not equally distributed on these two kinds of donor molecules. The **F** and **B** molecules individually formed head-to-tail pairs, which stacked alternately to form a [0, +1, +1, 0] CO pattern in the column (Figure 2a). The small overlap

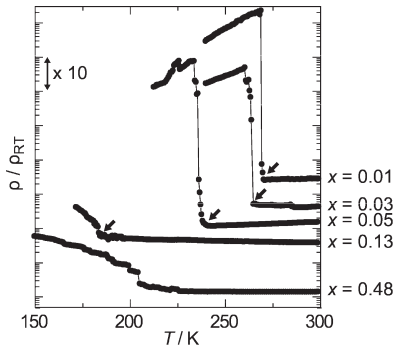

Figure 3. Temperature dependence of resistivities normalized with those at room temperature (ρ/ρ_{RT}) measured for single crystals of (Me_xEDO-TTF)$_2PF_6$ ($x \leq 0.48$). Samples for X-ray and conductivity measurements of $x = 0.03-0.48$ alloys were carved from the same crystals. The ordinate was shifted in the vertical direction for each crystal to avoid the overlap of data points. All the data plotted were taken in the cooling process. Arrows indicate the on-set of phase transition (T_c). Temperature dependences of ρ values of $x = 0.01-0.13$ alloys at $T < T_c$ are not correct due to the cracks of crystals during phase transition.

integral of the **B**-**B** pair (s_3 = 14.4−14.5 vs s_1 = 46.5−46.7 × 10^{-3} of the **F**-**F** pair at 150 K; see also Table S11, Supporting Information) indicates that the column consists of a [**B**, **F**, **F**, **B**] tetramer and that the phase transition includes the Peierls instability. It is noteworthy that such a molecular deformation in the LT phase was not observed for the x = 0.13 alloy (batch 4), implying that donor molecules possessed a uniform +0.5 charge even in the LT phase (Figure 2b). In fact, the central C=C bonds in crystallographically independent two donor molecules showed the same bond lengths (1.380(6) Å for both molecules at 150 K). Overlap integrals within the donor stacks became close to each other (s_3 = 26.3, s_2 = −31.5, and s_1 = 32.3 × 10^{-3} at 150 K), indicating also that the suppression of tetramerization in the LT phase took place (Figure 2b). The x = 0.48 alloy (batch 8) did not exhibit any structural transitions, and the nearly uniform head-to-tail stack and rotational disorder of the PF_6 anion observed at 300 K were preserved down to 150 K (Figure 2c).

The incorporation of MeEDO-TTF into (EDO-TTF)$_2PF_6$ suppressed all three phase transition mechanisms of this salt. Especially, the CO feature among the multi-instabilities was strongly suppressed as x increased and seemed to disappear in the x = 0.13 alloy. Alloying effects on the Peierls and AO instabilities were regarded to be smaller than that on the CO one.

Transport and Magnetic Properties. Figure 3 illustrates the temperature dependence of resistivities of EDO-TTF rich alloys measured for the single crystal samples (E// stacking direction). Similarly to (EDO-TTF)$_2PF_6$, all alloys exhibited a metallic or nearly constant resistivity around room temperature with room temperature conductivities of 10^1-10^2 S cm^{-1}. The $x \leq 0.13$ alloys showed a sharp M-I transition on cooling. The transition temperature (T_c) showed a low-temperature shift from 279 to 188 K with increasing x values from x = 0 (pristine (EDO-TTF)$_2PF_6$) to 0.13, and the transition became gradual. The x = 0.2−0.5 alloys also exhibited metallic behavior around room temperature. Below the temperature

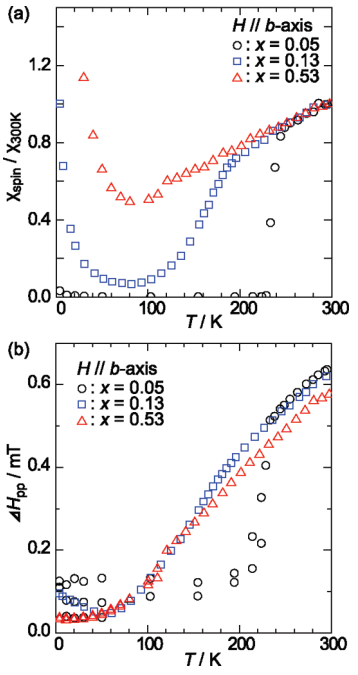

Figure 4. Temperature dependences of (a) spin susceptibilities (χ_{spin}) normalized with those of 300 K and (b) line widths (ΔH_{pp}) of (Me_xEDO-TTF)$_2PF_6$ (x = 0.05 (black circles, batch 3), 0.13 (blue squares, batch 4), and 0.53 (red triangles, batch 9)) in the ESR spectra measured for single crystals.[26]

at which the conductivity maximum was observed ($T_{\sigma max}$), the alloys showed a semiconducting behavior without an abrupt anomaly (for x = 0.48 in Figure 3, jumps were caused by cracking of the crystal). The $T_{\sigma max}$ value varied in the range of 200−270 K from crystal to crystal not only due to the variation of the x value but also due to the crystal quality (see also Figure S2, Supporting Information).

Figure 4 depicts the temperature dependences of spin susceptibilities (χ_{spin}) and line widths (ΔH_{pp}) of x = 0.05, 0.13, and 0.53 (batches 3, 4, and 9) alloys measured by the ESR technique. In the HT region, a Pauli-like paramagnetism was observed for all salts, consistent with their metallic behavior. The χ_{spin} of the x = 0.05 alloy sharply decreased to provide a diamagnetic state at 230−240 K, which is close to T_c (= 242 K) in the conductivity measurement (Figure 4a, black circles). The ΔH_{pp} also showed a rapid decrease at T_c (Figure 4b, black circles). In the case of the x = 0.13 alloy, the χ_{spin} value gradually decreased below ~185 K with an upturn below ~80 K due to the contribution of the impurity spin (Figure 4a, blue squares). The slope of ΔH_{pp} also became slightly larger at T_c (Figure 4b, blue squares). The x = 0.53 alloy did not show any anomalies, and both χ_{spin} and ΔH_{pp} monotonically decreased on cooling (Figure 4, red triangles), which is consistent with the absence of structural transition.

Raman Spectra. To investigate the CO behavior on donor molecules, temperature-variable Raman spectroscopy measurements were performed. Figure 5 shows the spectra of C=C stretching modes of x = 0.05 (batch 3), 0.13 (batch 4), and 0.52−0.54 (batch 9) alloys at 300 K and 7 or 8 K (see also Figures S4−S6, Supporting

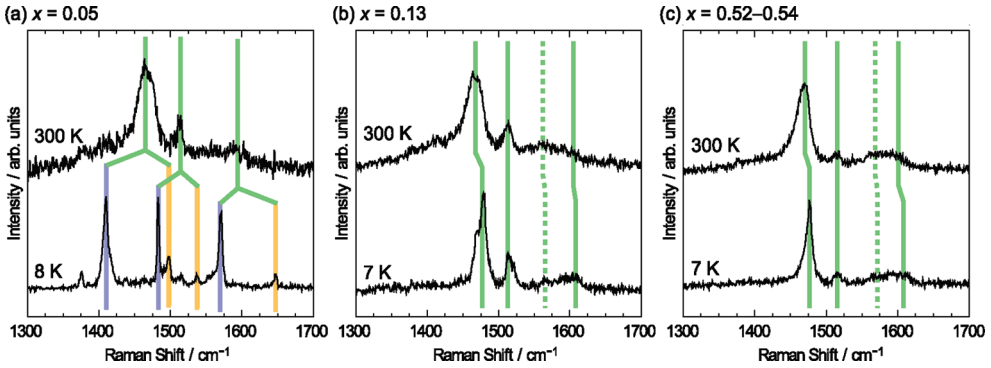

Figure 5. Raman spectra of $(Me_xEDO\text{-}TTF)_2PF_6$ of (a) $x = 0.05$ (batch 3), (b) $x = 0.13$ (batch 4), and (c) $x = 0.52-0.54$ (batch 9) at 300 K and 7 or 8 K excited by a He−Ne laser (633 nm). Bands of EDO-TTF having 0, +0.5, and +1 charges are indicated by orange, green, and blue solid lines, respectively, and that most plausibly assigned to MeEDO-TTF having a +0.5 charge is indicated by the green dotted line.

Information). These alloys at 300 K showed three bands at 1464−1470, 1512−1518, and 1590−1600 cm^{-1}, which are very similar to those of $(EDO\text{-}TTF)_2PF_6$ (1472, 1515, and ~1592 cm^{-1}) in the HT phase, suggesting that the donor molecule possesses a uniform +0.5 charge also in the alloys (Figure 5).[27] Although the Raman spectrum of +0.5 charged MeEDO-TTF has not been observed yet, the weak bands at 1550−1560 cm^{-1} detected in the $x = 0.13$ and 0.52−0.54 alloys may be assigned to the C=C stretching mode of $MeEDO\text{-}TTF^{0.5+}$ in comparison with the spectra of neutral and +1.0 charged radical cation species (indicated by green dotted lines in Figure 5b and c).[17] Another band of MeEDO-TTF (~1450 cm^{-1}) should overlap with that of the EDO-TTF molecule. These bands were not observed clearly in the $x = 0.05$ alloy probably due to too small a mole fraction of MeEDO-TTF. In the LT phase, the spectrum of the $x = 0.05$ alloy split into six peaks assignable as charge-poor (1497, 1537, and 1647 cm^{-1}, orange solid lines) and charge-rich (1410, 1483, and 1571 cm^{-1}, blue solid lines) EDO-TTF species (Figure 5a).[27] The spectral features of $x = 0.13$ and 0.52−0.54 alloys at 300 K were preserved even at 7 K, indicating that these alloys did not exhibit CO (Figure 5b and c). The CO state in the $x = 0.05$ alloy and the uniform +0.5 charge in the $x = 0.13$ and 0.52−0.54 alloys in the LT region well coincide with the molecular deformation and preservation of nearly flat molecules in the crystal structure analyses, respectively.

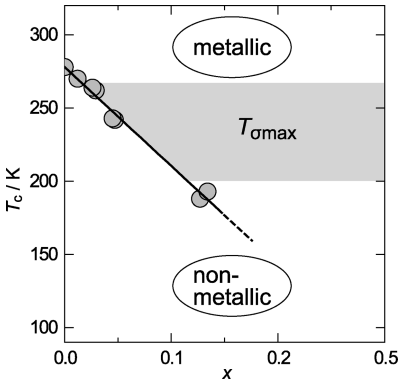

Figure 6. Mole fraction (x) dependence of the critical temperature between phenomenological metallic and nonmetallic behaviors (T_c) of EDO-TTF rich alloys ($x \leq 0.5$). T_c of $x \leq 0.13$ alloys was determined by the conductivity measurement. Note that the transition mechanism consists of Peierls, AO, and CO instabilities in the case of $x \leq 0.05$, while that for the $x = 0.13$ alloy contains only the former two instabilities. The temperatures for the maximum conductivity ($T_{\sigma max}$), which showed strong dependence on crystal quality, are approximately indicated by painting in gray.

Effects of Alloying. Figure 6 shows the phenomenological border between metallic and nonmetallic states of $(Me_xEDO\text{-}TTF)_2PF_6$ ($x \leq 0.5$). T_c proportionally decreases with increasing x value for the region of $x \leq 0.13$ despite the fact that the transition mechanism of $x = 0.13$ was different from those of $x \leq 0.05$. Alloying $(Me_xEDO\text{-}TTF)_2PF_6$ is expected to affect following four parameters: (1) amount of defects in the crystal, (2) site-charge distribution due to the ionization potential difference between EDO-TTF and MeEDO-TTF molecules, (3) intralayer (donor−donor) interactions, and (4) interlayer (donor−anion) interactions. As for parameter 1, it has been known that defects produced by an impurity causes the low-temperature shift and broadening of a first-order phase transition.[28] Also in the cases of low-dimensional organic conductors, impurity and positional disorder in a conduction column prevent the perfect nesting of the Fermi surface, resulting in the suppression and smearing of the Peierls transition.[29] The random distribution of MeEDO-TTF in

(26) The signal of $x = 0.05$ alloy in the LT phase ($T < 220$ K), which probably originates from the defect spins, showed a multiple signal feature. In the case of the $x = 0.53$ alloy, the signal was fitted with two Lorentzian signals at $T < 130$ K. Although the origin of the splitting is not clear yet, the two-signal feature was observed at room temperature in the angular dependent measurement (see Figure S3, Supporting Information). Temperature-variable measurement was performed applying the magnetic field parallel to the b-axis at which the difference of g-factors of these two signals was minimized. In this case, the observed signal could be represented with one Lorentzian model in the simulation. Because of signal sharpening, however, the two-signal feature was observed in the low-temperature region, and the simulation employing a couple of Lorentzians was needed. The χ_{spin} value was obtained by the sum of double integrations of the fitting curves, and ΔH_{pp} of each fitting curves are plotted in Figure 4b.

(27) Drozdova, O.; Yakushi, K.; Yamamoto, K.; Ota, A.; Yamochi, H.; Saito, G.; Tashiro, H.; Tanner, D. B. *Phys. Rev. B* **2004**, *70*, 075107/1–075107/8. For the spectra taken at 300 K, the bands observed for the $x = 0.05$ alloy at 1464, 1512, and ~1600 cm^{-1} correspond to the ones denoted as ν_γ, ν_β, and ν_α in this reference, and ν_6, ν_5, ν_4 in ref 9, respectively.

(28) Levanyuk, A. P. *Phase Transitions* **2003**, *76*, 253–259.

(29) Ishiguro, T.; Yamaji, K.; Saito, G. *Organic Superconductors*, 2nd ed.; Fulde, P., Ed.; Springer Series Solid-State Science 88; Springer: Berlin, Germany, 1998; Chapter 11.2.1, pp 403−406.

the conduction column and positional disorder of the methyl group should reduce the Peierls instability of the alloys and play an important role in the low-temperature shift and smearing of the M-I transition. Parameter 2 should not have a large effect on the charge-distribution in the donor stack since the difference of ionization potentials between EDO-TTF and MeEDO-TTF (+0.39 and +0.36 V vs SCE in cyclic voltammetry measurements, respectively)[16] is much smaller than the band widths of the resulting alloys (~1.3 eV). In fact, the Raman spectra did not exhibit the inhomogeneity of charges on EDO-TTF and MeEDO-TTF molecules (Figure 5). The overlap integrals within the conduction layer of $x \leq 0.13$ alloys in the HT phase varied slightly and nonsystematically (Table S10, Supporting Information), and those in the LT phase (x = 0.03 and 0.05 alloys, Table S11 (Supporting Information)) were close to each other. In accordance with these valuations, the valence-conduction band gaps calculated for the crystal structures of pristine $(EDO\text{-}TTF)_2PF_6$, x = 0.03, and 0.05 alloys at 150 K were 0.35, 0.34, and 0.33 eV, respectively, where the molecular shape dependence of orbital energy was concerned. This means that the band gap is hardly affected by the mole fraction of MeEDO-TTF at least in the range of CO takes place. Accordingly, the variation of intralayer interactions (parameter 3) would not be an origin of the decrease of T_c. Here, we focused on parameter 4, the donor−anion interaction. For the pristine $(EDO\text{-}TTF)_2PF_6$, the uniaxial strain experiments revealed that the strain along the interlayer direction, which shortens the donor−anion distance and strengthens the donor−anion interaction, most effectively enhanced T_c ($\Delta T_{MI} > +60$ K, 4 kbar).[8] The accurate structure analysis at ambient pressure showed that the M-I transition causes a displacement of the anion, resulting in the shortening of the distance between the anion and positive-charge rich S atom of the ionized donor molecule in the LT phase.[7] These preceding investigations suggest the importance of the electrostatic interaction between donor and anion molecules. The significance of attractive Coulomb interaction has also been claimed in other CO systems.[30]

Figure 7 illustrates the changes in cell parameters a (~side-by-side)-, b (stacking)-axes, and $V/(ab \sin \gamma)$ (interlayer distance) depending on the x value (Δa, Δb, and $\Delta V/(ab \sin \gamma)$, respectively). The lengths of a- and b-axes slightly increased according to the x value, although their scatterings were remarkable. To the contrary, $V/(ab \sin \gamma)$ exhibited an obvious and significant increment almost proportionally to x. Since the conduction and anion layers are composed of the π-electron system of the donor molecule (central TTF skeleton) and PF_6 in all alloys, respectively, the effective thickness of these layers do not depend on x. Accordingly, the extension of the unit cell along the interlayer direction ($V/(ab \sin \gamma)$) according

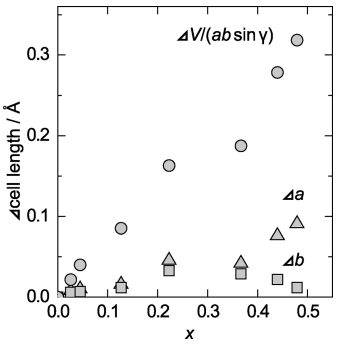

Figure 7. Changes in cell lengths depending on the x value in $x \leq 0.48$ alloys at room temperature or 300 K. Δa, triangles; Δb, squares; and $\Delta V/(ab \sin \gamma)$, circles.

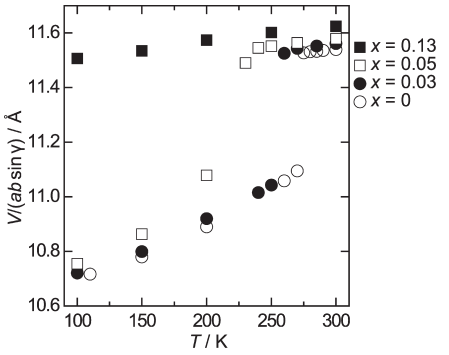

Figure 8. Temperature dependences of $V/(ab \sin \gamma)$ of EDO-TTF rich alloys ($x \leq 0.13$). x = 0, ○; x = 0.03, ●; x = 0.05, □; and x = 0.13, ■. $V/(ab \sin \gamma)$ of the LT phase was obtained by the conversion of its cell parameters.

to the x value corresponds to the increment of the effective donor−anion distance (separation between the conduction path and counteranion). This means that the incorporation of MeEDO-TTF kept the π-electron system of donor molecules away from PF_6 anions due to the steric hindrance of the methyl group, resulting in the weakening of electrostatic interaction between the conduction path and anions. Such an effect reduces the Coulomb stabilization energy of the LT phase, resulting in the lowering of T_c and further the disappearance of CO state in the x = 0.13 alloy. This result indicates that the electrostatic interaction between donors and anions plays an important role in the M-I transition of the present system. Figure 8 depicts the temperature dependences of $V/(ab \sin \gamma)$ of x = 0.03, 0.05, and 0.13 alloys together with that of pristine $(EDO\text{-}TTF)_2PF_6$ (x = 0), which corresponds to the temperature dependences of the effective donor−anion distance. The $V/(ab \sin \gamma)$ of x = 0−0.05 alloys abruptly decreased at the temperature of the M-I transition indicating the synchronous modulation of the lattice and the valence-conduction band gap. Interestingly, as shown by the closed squares in Figure 8, $V/(ab \sin \gamma)$ of the x = 0.13 alloy, which did not show the CO state in the LT phase, decreased smoothly compared with that in the x = 0 and 0.03 alloys. This result implies that the alloying weakened not only the electrostatic interaction but also the electron−phonon interaction to suppress the Peierls instability and to reduce the

(30) (a) Zorina, L.; Simonov, S.; Mézière, C.; Canadell, E.; Suh, S.; Brown, S. E.; Foury-Leylekian, P.; Fertey, P.; Pouget, J.-P.; Batail, P. *J. Mater Chem.* **2009**, *19*, 6980–6994. (b) Ota, A.; Ouahab, L.; Golhen, S.; Yoshida, Y.; Maesato, M.; Saito, G.; Świetlik, R. *Chem. Mater.* **2007**, *19*, 2455–2462.

valence-conduction band gap in the LT phase. In the pristine (EDO-TTF)$_2$PF$_6$, the structural fitness allowing the deformation of the donor molecule and the displacement of the anion into the donor layer increases the electrostatic stabilization of the LT phase and enhances the M-I transition.[7] This result suggests that the abrupt decrease of the effective donor−anion distance in the phase transition occurs to obtain the electrostatic stabilization of the CO state, and hampering such a structural fitness due to the steric effect of methyl group is also one of the origins of suppression of the M-I transition.

Elongation of the donor−anion distance reduces not only electrostatic interaction but also interatomic interactions such as the hydrogen bond, which is well known to regulate molecular packing in the organic crystals.[31] In the crystal structure of (EDO-TTF)$_2$PF$_6$, several C−H···F hydrogen bonds between the vinyl proton on EDO-TTF and the PF$_6$ anion are observed.[6] These interactions prevent the PF$_6$ anion from free rotation. The methyl substitution of (EDO-TTF)$_2$PF$_6$ interrupts the formation of C(sp^2)−H···F hydrogen bonds, which are stronger than C(sp^3)−H···F hydrogen bonds due to the larger polarity.[32,33] Furthermore, the extension of the donor−anion distance makes C−H···F hydrogen bonds longer and weaker. These effects cause the increase of freedom of anion rotation and would prevent the AO state. The fact that the thermal factors of F atoms in PF$_6$ anion in the LT phase increased with x value (averaged thermal factors; 0.0326 for $x = 0$ at 110 K, 0.0333 for $x = 0.03$, 0.0392 for $x = 0.05$, and 0.0846 for $x = 0.13$ at 100 K) in comparison with those of S atoms (averaged thermal factors; 0.0198 for $x = 0$ at 110 K, 0.0209 for $x = 0.03$, 0.0228 for $x = 0.05$, and 0.0231 for $x = 0.13$ at 100 K) supports this hypothesis. Hydrogen bond interaction is also regarded as an important factor to modulate charge distribution in the crystal structure (charge-pinning).[30a,34] Weakening C−H···F hydrogen bonds by methyl substitution would also prevent the CO state in the present system.

In the case of the $x \sim 0.5$ alloy, too much extension of the donor−anion distance would prevent both CO and AO states, where uniform +0.5 charge on donor molecule was preserved not to open the valence-conduction band gap even in the low-temperature region, and that can be regarded as one of the origins of absence of any abrupt phase transitions in this alloy. The appearance of conductivity maxima ($T_{\sigma max}$ = 200−270 K) for $x \geq 0.13$ alloys would be caused by the damages on crystal or crossover-like transition to a narrow gap semiconductor.

2. MeEDO-TTF Rich Salts ($x \geq 0.91$). *Crystal Structures*. Crystallographic data of an MeEDO-TTF rich alloy ($x = 0.94$, batch 11), which was isostructural to pristine (MeEDO-TTF)$_2$PF$_6$ for both HT and LT phases, are listed in Table 3 (see also Tables S8 and S9, Supporting Information for other $x \geq 0.91$ alloys). Distinguishable differences in cell lengths (>0.02 Å) were not observed by the incorporation of an EDO-TTF molecule in comparison with those of EDO-TTF rich alloys even for the $x = 0.91$ alloy (Table S8, Supporting Information). In the HT phase, the asymmetric unit contained one donor molecule and a half of the PF$_6$ anion which showed a significant disorder. The methyl group showed no positional disorder when s.o.f. was assumed to correspond to the result of EI-MS measurement, and any ordering between EDO-TTF and MeEDO-TTF was not observed in the donor sites. The donor molecules laid on the mirror planes at $z = 1/4$ and 3/4 and interacted with each other along the side-by-side direction (b-axis) (Figures 9a and 10a). A head-to-head stack with a small overlap and ~5° of twisting of molecular long axes was observed along the c-axis to establish a two-dimensional structure (Figure 10b). Overlap integrals within the donor layer calculated by the extended Hückel method were relatively small ($< 10 \times 10^{-3}$, Figure 10a) and close to those of pristine (MeEDO-TTF)$_2$PF$_6$ ($c = -9.9$, $p = 8.5$, and $s = 4.9 \times 10^{-3}$).[17] At lower temperature, the alloy showed a structural transition accompanying a change in the space group from *Cmcm* to *Pbcn*. The most significant difference in the donor layer between HT and LT phases was the dihedral angle between the best planes of neighboring donor molecules along the b-axis (0° at 300 K and 4.4° at 250 K; $x = 0.94$, Figure 9b and c). These structural features are also observed for pristine (MeEDO-TTF)$_2$PF$_6$.[17]

Table 3. Crystallographic Data of the $x = 0.94$ Alloy (Batch 11) at 300 and 250 K[a]

T (K)	300 K	250 K
crystal system	orthorhombic	orthorhombic
space group	*Cmcm*	*Pbcn*
a (Å)	29.662(3)	29.459(4)
b (Å)	12.615(2)	12.607(2)
c (Å)	6.994(0.5)	6.947(0.5)
V (Å^3)	2617.1(4)	2580.0(6)
Z	4	4
no. of unique refln.	1447	2288
no. of used refln.	1072	1575
no. of params	121	169
R ($I > 2\sigma(I)$)	0.0696	0.0739
$wR2$ (all data)	0.2183	0.2062
GOF	1.074	1.009

[a] For more data including ones at 200 and 110 K, see Supporting Information.

Transport and Magnetic Properties. Temperature dependence of resistivities of $x \geq 0.91$ alloys are shown in Figure 11. Alloys in the HT phase showed a semiconducting behavior with the conductivity of $\sim 10^0$ S cm^{-1} and activation energy of 110−220 meV, the latter of which was significantly higher than that of pristine (MeEDO-TTF)$_2$PF$_6$ (34 meV at 305 K).[17] The higher activation energy in the HT phase might be caused by the coexistence of nearly localized CD and distinct CD states as described below. A semiconductor-to-semiconductor phase transition accompanying a rapid increase of resistivity was observed for all alloys around room temperature.

(31) Fourmigué, M.; Batail, P. *Chem. Rev.* **2004**, *104*, 5379–5418.
(32) Gu, Y.; Kar, T.; Scheiner, S. *J. Am. Chem. Soc.* **1999**, *121*, 9411–9422.
(33) Scheiner, S.; Grabowski, S. J.; Kar, T. *J. Phys. Chem. A* **2001**, *105*, 10607–10612.
(34) Bandrauk, A. D.; Ishii, K.; Truong, K. D.; Aubin, M.; Hanson, A. W. *J. Phys. Chem.* **1985**, *89*, 1478–1485.

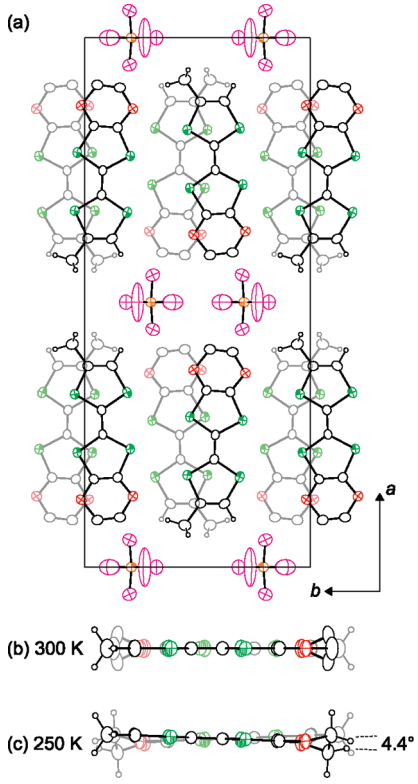

Figure 9. (a) Crystal structure of MeEDO-TTF rich alloy (x = 0.94, batch 11) at 300 K viewed along the c-axis. Light and deep colored molecules lie on the mirror planes at z = 1/4 and 3/4, respectively. (b and c) Projections of two neighboring donor molecules along the b-axis at 300 and 250 K, respectively.

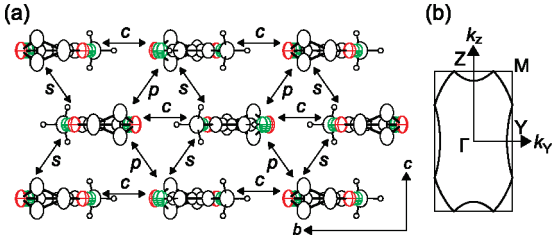

Figure 10. (a) Donor layer of $(Me_xEDO\text{-}TTF)_2PF_6$ (x = 0.94, batch 11) at 300 K viewed along the molecular long axis (a-axis). Letters present intermolecular overlap integrals, values of which were calculated by the extended Hückel method as c = 9.9, p = 8.7, and $s = -4.9 \times 10^{-3}$. (b) Calculated Fermi surface at 300 K.

The activation energy in the LT phase decreased with lowering temperature reaching 150−200 meV at 240 K, similar to that of pristine $(MeEDO\text{-}TTF)_2PF_6$ (see Figure S7). T_c decreased proportionally with decreasing x values from T_c = 303 K of pristine $(MeEDO\text{-}TTF)_2PF_6$ to 284 K of x = 0.91 alloy (Figure 12). The transition also became gradual with decreasing x values. The hysteresis loop observed in pristine $(MeEDO\text{-}TTF)_2PF_6$ was not clearly found for the alloys due to the broadening of transition.

Figure 13 illustrates the temperature dependences of χ_{spin} and ΔH_{pp} of an alloy crystal from batch 11 (x = 0.92−0.94) measured by the ESR technique. In the HT phase, χ_{spin} decreased with lowering temperature and increased rapidly at the on-set temperature of phase transition (~290 K). While some scatter was observed, χ_{spin} in the LT phase gradually decreased with temperature. The

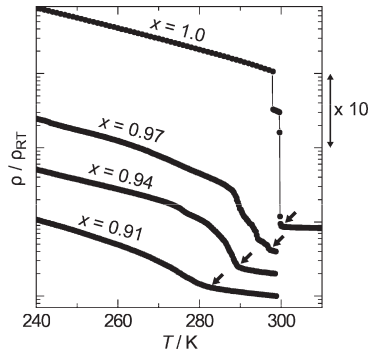

Figure 11. Temperature dependence of resistivities measured for single crystals of $(Me_xEDO\text{-}TTF)_2PF_6$ ($x \geq 0.91$) normalized with those at room temperature (ρ/ρ_{RT}). The ordinate was shifted in the vertical direction for each x to avoid the overlap of data points. Arrows indicate the on-sets of phase transition.

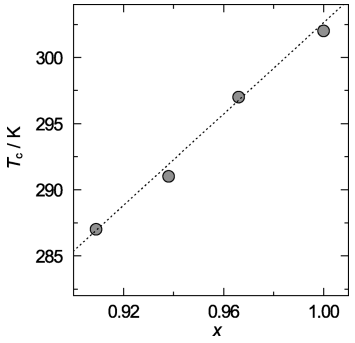

Figure 12. Plot of T_c for $x \geq 0.91$ alloys and $(MEEDO\text{-}TTF)_2PF_6$ vs mole fraction (x). T_c was determined by conductivity measurement.

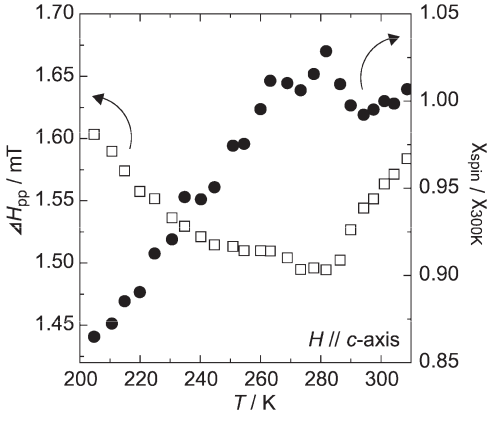

Figure 13. Temperature dependences of χ_{spin} normalized with that of 300 K (●) and ΔH_{pp} (□) of an alloy of batch 11 (x = 0.92−0.94).

temperature dependence of χ_{spin} of this alloy is very similar to that of the static magnetic susceptibility of pristine $(MEEDO\text{-}TTF)_2PF_6$ except for a broadening of the phase transition (280−290 K) in the present case. Similar to χ_{spin}, ΔH_{pp} decreased with lowering temperature in the HT phase. ΔH_{pp} increased gradually with lowering temperature in the LT phase.

Raman Spectra. In the Raman spectra of pristine $(MEEDO\text{-}TTF)_2PF_6$, C=C stretching modes are observed at 1456 and 1558 cm^{-1} at 310 K (HT phase), and 1531, 1561, and 1625 (weak) cm^{-1} at 100 K (LT phase).[17] In addition, the LT phase shows a very broad band at the

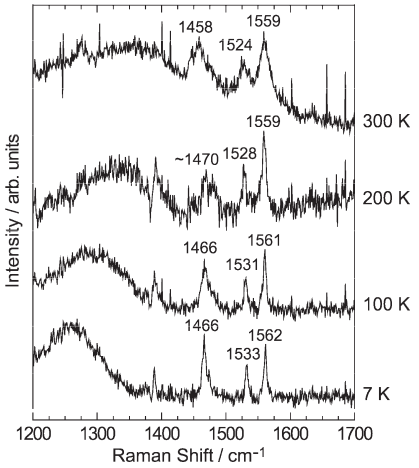

Figure 14. Temperature-variable Raman spectra from an alloy crystal of batch 11 ($x = 0.92-0.94$). The Raman shift for each band discussed in the text is indicated in units of cm^{-1}.

lower energy region which distinctly shifts from ~1400 cm^{-1} (300 K) to ~1300 cm^{-1} (100 K) with lowering temperature. Figure 14 shows the temperature-variable Raman spectra measured for an alloy of batch 11 ($x = 0.92-0.94$). In the HT phase ($T = 300$ K), there were three bands at 1458, 1524, and 1559 cm^{-1} and a broad band at 1200−1420 cm^{-1}, which are assignable as C=C stretching modes of the MeEDO-TTF molecule. The spectrum can be explained by the superimposition of those of $(MeEDO-TTF)_2PF_6$ in the HT and LT phases,[17] indicating the coexistence of the nearly localized CD and distinct CD states. To understand the origin of this concomitant behavior, it is suggested that the incorporation of EDO-TTF molecule generates a trapping site, which suppresses the fluctuation of charges on donor molecules. Since the steric hindrance of the methyl group is reduced, the donor molecule and anion would become closer to each other and interact more strongly at the trapping site, resulting in the suppression of the spatial fluctuation of the CD state in the vicinity of EDO-TTF occupied sites. However, the C=C stretching modes observed at $T \leq 250$ K were similar to those of pristine $(MeEDO-TTF)_2PF_6$ in the LT phase except for an additional band at ~1470 cm^{-1}, indicating the distinct CD state of this alloy. Although complete assignment has not been performed, the additional band at ~1470 cm^{-1} is speculated as the ν_{13} and ν_{15} modes, which are much weaker in pristine $(MeEDO-TTF)_2PF_6$, enhanced by the disorder in the crystal.[17]

Effects of Alloying. The phase transition of $(MeEDO-TTF)_2PF_6$ type alloys ($x \geq 0.91$) showed a low-temperature shift and dull feature as x decreased (increasing the mole fraction of EDO-TTF). Among the effects (1)−(4) of alloying described before, parameter 2 should be ignorable because of the similar ionization potentials between EDO-TTF and MeEDO-TTF. The effect of parameter 3 would also be negligible since the overlap integrals in the donor layer in both HT and LT phases were very similar to those of pristine $(MeEDO-TTF)_2PF_6$ (Table S12, Supporting Information). Figure 15 plots the changes in the cell parameters, a (interlayer)-, b (side-by-side)-, and

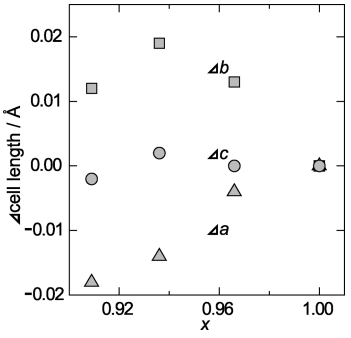

Figure 15. Changes in cell lengths depending on x value for MeEDO-TTF rich alloys ($x \geq 0.91$). Δa, triangles; Δb, squares; and Δc, circles.

c (stacking)-axes depending on the x value for the HT phase at room temperature (Δa, Δb, and Δc, respectively). Within the conduction layer, the c-axis length was nearly constant, and the b-axis length became slightly longer with decreasing x values. Along the interlayer direction, the a-axis length became shorter with decreasing x values, suggesting the suppression of steric hindrance by the reduction of the methyl group ratio. Differences of the interlayer distance ($\Delta a/2$) which correspond to the effective donor−anion distance in $x \geq 0.91$ alloys were smaller than the $\Delta V/(ab \sin \gamma)$ values of EDO-TTF rich alloys ($\Delta a/2 = 0.007$ Å for $x = 0.94$, and $\Delta V/(ab \sin \gamma) = 0.04$ Å for $x = 0.05$) (Figures 7 and 15). Although compression of the donor−anion distance is expected to enhance the phase transition due to the intensification of donor−anion interactions, the phase transition was suppressed by the incorporation of the EDO-TTF molecule. Accordingly, the lattice modulation to shorten the donor−anion distance should have a negligible effect on the phase transition of MeEDO-TTF rich alloys. However, as described in the temperature dependence of Raman spectra, it was suggested that the removal of the methyl group generates stronger donor−acceptor interaction sites, where CD is locally enhanced, and the site-charge fluctuation is suppressed. This effect is regarded as causing the coexistence of the nearly localized CD and distinct CD states and also the increment of activation energy in the HT phase. As for the low-temperature shift and broadening of the phase transition, the defect increased by alloying and random distribution of EDO-TTF in the conduction layer (parameter 1) would have the most significant effect.

Conclusions

Alloyed salts between EDO-TTF and MeEDO-TTF, $(Me_xEDO-TTF)_2PF_6$, with mole fractions of $0 < x < 1$ were successfully prepared, despite the differences in molecular shapes and physical properties of their pristine PF_6 salts. The x values for EDO-TTF rich alloys ($x \leq 0.5$) were nearly consistent with the donor mixing ratio in the reaction mixture. EDO-TTF rich alloys were isostructural to pristine $(EDO-TTF)_2PF_6$, and EDO-TTF and MeEDO-TTF molecules were randomly arranged in the head-to-tail stack. Alloys obtained from an MeEDO-TTF rich mixture contained a large excess amount of MeEDO-TTF

($x \geq 0.91$) and were isostructural to pristine (MeEDO-TTF)$_2$PF$_6$. The alloys having mole fractions of $0.6 < x < 0.9$ were not obtained.

Incorporation of MeEDO-TTF into (EDO-TTF)$_2$PF$_6$ anisotropically extended the lattice constants. Along the molecular long axis (interlayer direction), the unit cell was most effectively extended due to the steric effect of the methyl group, which means the extension of the donor−anion distance. Alloying the donor molecules effectively modulated the physical properties of the (EDO-TTF)$_2$PF$_6$ system; the M-I transition was suppressed, resulting in the lowering of T_c and smearing of the phase transition in the low x region, and the absence of abrupt transition in higher x alloys ($> \sim 0.2$). Extension of the donor−anion distance which weakens donor−anion interactions (electrostatic stabilization and hydrogen bond) is regarded as significantly suppressing CO instability. The disorder generated by the incorporation of MeEDO-TTF and the hampering of structural fitness are also important factors for the low-temperature shift and smearing of the M-I transition. The most striking feature of EDO-TTF rich alloys is the selective elimination of the CO instability in the $x = 0.13$ alloy, for which the abrupt lattice modulation associated with the M-I transition of $x \leq 0.05$ alloys also vanished.

Also in the MeEDO-TTF rich alloys ($x \geq 0.91$), EDO-TTF and MeEDO-TTF molecules were randomly arranged in the conduction layer. On the basis of the crystal structure analysis, conductivity measurement, and ESR spectra, these alloys exhibited a semiconductor-to-semiconductor phase transition similar to that of pristine (MeEDO-TTF)$_2$PF$_6$. This phase transition showed a low-temperature shift and broadening according to the mole fraction of EDO-TTF most probably due to the defect effect. The coexistence of nearly localized CD and distinct CD states in the HT phase suggests that EDO-TTF molecule plays a role of a trapping site preventing the fluctuation of CD in the conduction layer by the generation of stronger donor−anion interaction sites.

We emphasize that our study of alloying two phase transition systems, namely PF_6 salts of pristine and methylated EDO-TTF extracted the importance of donor−anion interaction to these peculiar phase transition systems. Furthermore, the EDO-TTF rich alloys demonstrated the selective annihilation of CO instability among the cooperative phase transition mechanisms in (EDO-TTF)$_2$PF$_6$. Along with the coexistence of two kinds of CD states observed in MeEDO-TTF rich alloys, the tuning of multi-instabilities is realized in the (Me$_x$EDO-TTF)$_2$PF$_6$ alloys studied here. The results will contribute to the understanding of the dynamic process of a multi-instability system and establish a designing strategy for functional materials exhibiting peculiar phase transitions.

Acknowledgment. This work was partly supported by Grants-in-Aid for Scientific Research on Innovative Areas (20110006) from the Ministry of Education, Culture, Sports, Science and Technology, Japan, for Creative Scientific Research (18GS0208) from the Japan Society for the Promotion of Science (JSPS), and for the Joint Studies Program (2008−2009) of the Institute for Molecular Science.

Supporting Information Available: Photographs of crystals, crystallographic data, overlap integrals calculated by the extended Hückel method, temperature dependences of resistivity and Raman spectra of EDO-TTF rich alloys, temperature and angular dependences of ESR spectra of the $x = 0.53$ alloy, and temperature dependence of activation energy of MeEDO-TTF rich alloys in PDF format, and crystal data in CIF format. This material is available free of charge via the Internet at http://pubs.acs.org.